LANGMUIR

pubs.acs.org/Langmuir Article

The Assembly Mechanism and Mesoscale Architecture of Protein—Polysaccharide Complexes Formed at the Solid—liquid Interface

Shanta Biswas, Laurence D. Melton, Andrew R. J. Nelson, Anton P. Le Brun, Frank Heinrich, Duncan J. McGillivray, and Amy Y. Xu*



Cite This: Langmuir 2022, 38, 12551-12561



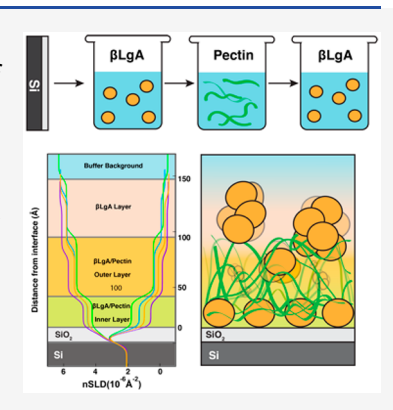
ACCESS I

III Metrics & More

Article Recommendations

Supporting Information

ABSTRACT: Protein—polysaccharide composite materials have generated much interest due to their potential use in medical science and biotechnology. A comprehensive understanding of the assembly mechanism and the mesoscale architecture is needed for fabricating protein—polysaccharide composite materials with desired properties. In this study, complex assemblies were built on silica surfaces through a layer-by-layer (LbL) approach using bovine beta-lactoglobulin variant A (β LgA) and pectin as model protein and polysaccharide, respectively. We demonstrated the combined use of quartz crystal microbalance with dissipation monitoring (QCM-D) and neutron reflectometry (NR) for elucidating the assembly mechanism as well as the internal architecture of the protein—polysaccharide complexes formed at the solid—liquid interface. Our results show that β LgA and pectin interacted with each other and formed a cohesive matrix structure at the interface consisting of intertwined pectin chains that were cross-linked by β LgA-rich domains. Although the complexes were fabricated in an LbL fashion, the complexes appeared to be relatively homogeneous with β LgA and pectin molecules spatially distributed within the matrix structure. Our results also demonstrate that the density



of β LgA-pectin complex assemblies increased with both the overall and local charge density of pectin molecules. Therefore, the physical properties of the protein-polysaccharide matrix structure, including density and level of hydration, can be tuned by using polysaccharides with varying charge patterns, thus promoting the development of composite materials with desired properties.

INTRODUCTION

Composite materials are formed by combining two or more materials with different physical and chemical properties. Composite materials can be found extensively in nature, ranging from natural wood to bones and connective tissues. Man-made composite materials can be traced back to the early days when ancient Egyptians mixed mud and straws to make bricks as building materials. In recent years, the fabrication of novel composite materials has always been an active area of research, through which materials with diverse and unique properties are developed and used in a wide range of applications that span from spacecraft to orthopedic implants. 3,4

Composite materials can be made from various components to suit different needs. Metals, ceramics, nanoparticles, synthetic polymers, and biopolymers are all popularly used to develop composites with desired properties including high mechanical strength, controlled porosity, low density, and excellent resistance to fatigue. The unique properties possessed by a composite material are not only related to the physical/chemical features of individual components but they can stem from the interactions and arrangements between individual components, leading to the formation of hierarchical assemblies with novel structural and mechanical properties.

In nature, proteins and polysaccharides coexist in almost all living biological systems. Phey can interact and form matrices surrounding living cells, leading to cohesive and functional biological structures. Such a structure is known as the extracellular matrix (ECM). Inspired by nature, composite materials consisting of proteins and polysaccharides have been developed for a wide range of biomedical applications including tissue engineering and drug delivery systems. The interactions and spatial arrangements of protein and polysaccharide molecules within the complex structure are critical in determining the macroscopic properties of such composite materials.

There are many ways to fabricate protein—polysaccharide composite materials, ranging from electrospinning and complex coacervation to film casting. ^{20–22} Of these methods, film casting via the LbL approach represents an easy but robust

Received: July 26, 2022 Revised: September 20, 2022 Published: October 4, 2022





method for fabricating protein—polysaccharide nanocomposites with tunable thickness and microstructures for desired applications.^{23–26} In the LbL approach, oppositely charged protein and polysaccharide molecules are alternatively adsorbed onto a solid substrate via electrostatic interactions,²⁷ leading to the formation of multilayered assemblies whose thickness can be easily controlled at the nanometer scale.²⁸

Characterizations of protein-polysaccharide composites are often focused on their morphological and mechanical properties at the macroscopic scale. 18,29 The ability to characterize the assembly mechanism of protein-polysaccharide composites will benefit the design and development of such materials by providing molecular-level information on the interactions and spatial arrangements of biomacromolecules as the building process proceeds. Motivated by this goal, this study demonstrates the combined use of quartz crystal microbalance with dissipation monitoring (QCM-D) and neutron reflectometry (NR) for characterizing the assembly mechanism of protein-polysaccharide matrices formed via the LbL approach, on a hydrophilic silica surface. New structures deposited onto the silica surface after each surface treatment was characterized in detail, and such information allows for better control of the mesoscale architectures of protein-polysaccharide matrices.

In this study, we chose bovine beta-lactoglobulin variant A (β LgA) and pectin as the model protein and polysaccharide, respectively. In particular, pectins with varying charge patterns were used to investigate if we could control the structure of protein-polysaccharide composite materials by tuning the electrostatic interactions between protein and polysaccharide molecules. For pectin samples, the degree of methylesterification (DM) determines the overall charge carried by the pectin molecules: the higher the DM, the less charge carried by the pectin molecule, and vice versa. The distribution pattern of the galacturonic acid (GalA) units along the pectin chain can be either random or block-wise. Therefore, the degree of blockiness (DB) is indicative of the local charge density of the pectin molecules: the higher the DB, the higher the local charge density of pectin. Collectively, DM and DB determine the overall and local charge densities carried by pectin, controlling the strength of electrostatic interactions between β LgA and pectin molecules. ^{21,30} QCM-D and NR measurements were made to characterize the assembly mechanism and structure of β LgA-pectin matrices formed on the silica surface in situ.

EXPERIMENTAL

Bovine beta-lactoglobulin variant A (β LgA) and pectin with 75% degree of methyl-esterification (75R) were purchased from Sigma-Aldrich (Missouri, US). Pectin with a 5% degree of methylesterification (5R) was purchased from Elicityl (Crolles, France). Pectins with a 37% degree of methyl-esterification were a gift from C.P. Kelco (Georgia, US). These pectin samples had been enzymatically de-esterified from highly methyl-esterified pectins using fungal and plant pectin methyl-esterase to create random and block-wise distributed methyl-ester groups (37R and 37B). Pectin samples were named as 5R, 37B, 37R, and 75R. The numbers indicate the degree of methyl-esterification, and the letters 'R' and 'B' denote a random or block distribution pattern of the methyl-ester groups (Figure 1). Pectin samples used in this study have molecular weights in the range from 90 to 120 kDa. The polydispersity index (PDI) of all pectin samples is expected to be around 2 based on results from a previous study.³¹ All other chemicals were of analytical grade from Sigma-Aldrich (Missouri, USA) and used without further purification. All samples were prepared in 5 mM citrate buffer at pH 4: β LgA and pectin were prepared at 5 and 1 mg/mL, respectively. To prepare a

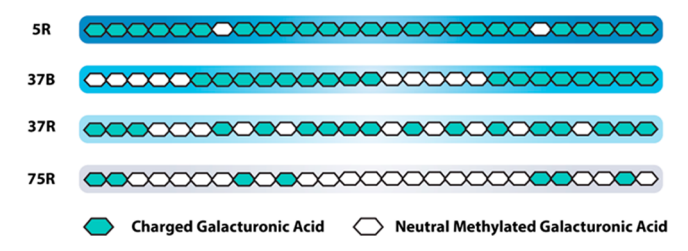


Figure 1. Illustration of pectins used in this study. The overall charge density of pectin decreases from SR to 75R with an increasing amount of methyl-esterification; 37B pectin has a higher local charge density than 37R since the charged galacturonic acid groups are arranged in blocks.

deuterated citrate buffer, D_2O was used instead of H_2O . The unit M stands for the molar concentration of mol/L, whereas mM stands for the concentration of 10^{-3} mol/L. Samples were allowed to hydrate overnight at 4 °C. All solutions were filtered through a 0.45 μ m PTFE syringe filter before use.

Quartz Crystal Microbalance with Dissipation Monitoring (QCM-D). QCM-D is a sensitive surface characterization technique that utilizes the piezoelectric property of quartz crystals to measure adsorbed mass with a subnanogram resolution. Deposition of mass onto the crystal surface leads to a decrease in the resonant frequency, F. If a thin and rigid film of mass is adsorbed onto the crystal surface, then the relationship between the adsorbed mass (Δm) and the change in oscillating frequency (ΔF) can be expressed by Sauerbrey equation: 32,33

$$\Delta m = -\frac{C}{n}\Delta F\tag{1}$$

where n is the harmonic or overtone number, and C is the mass sensitivity constant related to the thickness, density, and resonant frequency of the crystal. If the deposited material is viscoelastic, the crystal oscillation is damped, and the Sauerbrey equation is no longer valid. Instead, the energy dissipation of the crystal expressed by the dissipation factor D has to be taken into account:

$$D = \frac{1}{Q} = \frac{E_d}{2\pi E_s} \tag{2}$$

where Q is the quality factor of the crystal, E_d is the energy dissipated or lost during one oscillation cycle, and E_s is the total energy stored in the oscillating system.³⁴ In a typical QCM-D experiment, a decrease in frequency implies mass adsorption onto the quartz crystal. A small dissipation value suggests that the surface layer is dense and rigid, while a large dissipation value is indicative of a viscoelastic surface structure.

The assembly of β LgA/pectin complexes was monitored *in situ* by an E4 QCM-D instrument (Q-Sense, Gothenburg, Sweden). The instrument has a measurement platform consisting of four temperature-controlled flow cells, supporting four simultaneous measurements. All measurements were collected in batch mode at 25 °C. Sensor crystals coated with SiO2 were cleaned by soaking in 2% v/v Hellmanex (Hellma Analytics, NY, USA) solution for 20 min, followed by repetitive washing in ultrapure water. The sensor was dried by a gentle nitrogen flow and cleaned by UV-ozone for 20 min. Measurements were started by equilibrating the system with citrate buffer at a flow rate of 0.05 mL/min, with 5 mg/mL β LgA solution being introduced into the cell chamber when the baseline was stable. After adsorption equilibrium was reached, the system was flushed with 5 mM citrate buffer at pH 4. The same procedure was followed for the deposition of pectin and a subsequent layer of β LgA. During the entire process, changes in frequency and dissipation were recorded as a function of time. Adsorption was monitored from the third to the 11th overtone. The seventh overtone was used in interpreting the QCM-D data due to the minimal noise level.

Neutron Reflectometry (NR). Neutron reflectometry (NR) experiments were performed on the PLATYPUS time-of-flight

neutron reflectometer at ANSTO, Australia.³⁵ Neutron pulses were generated using a disk chopper system with 3.3% wavelength resolution. For all NR measurements, the 8 cm × 4 cm × 0.5 cm (100)-cut silicon wafers (EL-CAT Inc., NJ, USA) were cleaned by soaking in 5% Decon 90 (Decon Laboratories Limited, East Sussex, UK) solution for 3 h first. Right before NR measurements, the silicon wafers were cleaned in a UV-ozone oven for 20 min, rinsed with ultrapure water and propan-2-ol, and dried under nitrogen flow. Cleaned wafers were assembled into a custom-made fluid cell with 300 μ L of exchangeable backing solution reservoir adjacent to the sample surface. After assembly, 3 mL of the β LgA solution was injected into the fluid cell and incubated with the silica surface for 2 h until an equilibrium was reached. The β LgA solution was then replaced by injecting 10 mL of citrate buffer in H₂O, followed by NR measurement to characterize the surface in hydrogenated buffer background. After measurements were done in the hydrogenous buffer, citrate buffer in D₂O was injected into the wet cell, with the neutron reflectivity from the surface measured again. Therefore, after each surface treatment, two contrasts (H₂O and D₂O) were measured for each sample. The same procedure was followed for the deposition of pectin and another layer of β LgA. The neutron reflectivity R was measured at three different incidence angles: 0.65° (1.53 mm slit 2 and 0.55 mm slit 3), 2.5° (5.88 mm slit 2 and 2.12 mm slit 3), and 3.8° (8.94 mm slit 2 and 3.23 mm slit 3) covering a Q-range of 0.0079-0.3 Å⁻¹, where Q is the scattering vector $(Q = 4\pi \sin \theta/\lambda)$, where θ is the angle of incidence and λ the neutron wavelength). For each sample, reflectivity was measured for 600 s with the incident angle of 0.65°, 1800 s at 2.5°, and 7200 s at 3.8° to ensure good statistics.

Reflectivity data were reduced using the SLIM module from the MOTOFIT reflectometry analysis software.³⁶ The slab model was used to fit the reflectivity data.^{37,38} To this end, we considered each slab as a layer of the sample that could be characterized by a particular neutron scattering length density (nSLD) value, differing from adjacent regions along the z direction.³⁹ The structural information on deposited films was extracted from the reflectivity profile by corefining $\rm H_2O$ - and $\rm D_2O$ -based contrasts using the MOTOFIT 40 reflectometry analysis software. Utilizing multiple solvent contrasts lowers the uncertainty of the structural model and allows the degree of solvent penetration to be determined. ⁴¹ The nSLD values of H₂O, D2O, Si, and SiO2 were calculated using the SLD calculator implemented in MOTOFIT. Considering hydrogen-deuterium exchange, the nSLD value of β LgA was calculated to be 2.50 \times 10^{-6} Å^{-2} in deuterated buffer and $1.76 \times 10^{-6} \text{ Å}^{-2}$ in hydrated buffer (biomolecular scattering length density calculator, ISIS Neutron and Muon Source (http://psldc.isis.rl.ac.uk/Psldc/).42 Similarly, the nSLD values of various pectins were calculated using a method described in a previous study⁴³ (Table 1).

Table 1. Calculated nSLD Values of Pectins with Different Charge Densities

nSLD of pectin	5R	37R and 37B	75R
In D_2O (×10 ⁻⁶ Å ⁻²)	4.16	4.06	3.93
In H_2O (×10 ⁻⁶ Å ⁻²)	2.91	2.82	2.72

During the fitting process, the roughness of each layer was fixed at 4 Å. Other parameters, including thickness, nSLD value, and solvent percentage, were also included to describe each layer. The nSLD value of each layer is only related to the amount of β LgA and pectin present in that layer (i.e., no contribution from solvent), whereas solvent percentage accounts for the amount of water present in the layer. Since the nSLD value of a mixed layer reflects the amount of β LgA and pectin that coexist in that layer, the nSLD value could be used to calculate the percentage of β LgA and pectin in the mixed layer since the nSLD values of both macromolecules are known (eq 3):

$$nSLD = P_{\beta LgA} \times nSLD_{\beta LgA} + (1 - P_{\beta LgA}) \times nSLD_{pecti}$$
(3)

where $P_{\beta LgA}$ is the percentage of β LgA in the mixed layer, and the percentage of pectin is $1-P_{\beta LgA}$. Solvent percentage of each layer was determined through the fitting process, representing the volume fraction occupied by solvent in that layer. The percentages of β LgA and pectin in the mixed layer calculated from eq 3 were then converted to their corresponding volume fractions by taking the amount of solvent present in that layer into account (eq 4):

$$\begin{split} \phi_{\beta LgA} &= P_{\beta LgA} \times (1 - \phi_{solvent}) \\ \phi_{pectin} &= (1 - P_{\beta LgA}) \times (1 - \phi_{solvent}) \end{split} \tag{4}$$

where $\phi_{\beta LgA}$ and ϕ_{pectin} are the volume fractions of βLgA and pectin, respectively, in the mixed layer; $\phi_{solvent}$ is the solvent percentage obtained from the fitting process. For example, if solvent accounts for 30% of the layer, then βLgA and pectin together make up 70%. The volume fraction of βLgA and pectin can then be calculated by multiplying the percentage of each in the mixed layer by 70%. Collectively, the volume fraction of βLgA , pectin, and solvent have a sum of 100%. Surface coverage (Γ) of βLgA and pectin after each surface treatment was calculated using

$$\Gamma = \tau \phi \rho \tag{5}$$

where τ is the layer thickness in cm, ϕ is the volume fraction of β LgA or pectin, and ρ is the mass density of the corresponding macromolecule with the unit of g/cm³. The density of β LgA is ~ 1.32 g/cm³, whereas the density of pectin is ~ 1.75 g/cm³, according to previous research. ^{43,44}

For the same surface, two contrasts were measured by NR experiments: one in a hydrogenated buffer and the other in a deuterated buffer. For the mixed layer containing β LgA and pectin, the amount of protein and polysaccharide was expected to remain the same in both contrasts (since only the buffer was replaced between the two measurements). Therefore, a list of nSLD values was calculated and tabulated for a wide range of β LgA and pectin compositions for both contrasts. During the corefining process, the nSLD value of the mixed layer was set to a particular paired nSLD values (one for deuterated and one for hydrogenated buffer background) for a certain βLgA and pectin composition (Table S1). The nSLD values were allowed to vary in a narrow range for each contrast, thus ensuring the composition of the mixed layer remained constant in both buffer backgrounds. Different nSLD values were trialed, and the set of values given the lowest χ^2 values was recorded. The obtained structure parameters including thickness, nSLD value, and solvent percentage for each layer after each surface treatment are shown in Tables S2 and S3.

RESULTS AND DISCUSSION

Monitoring the Deposition of β LgA and Pectin onto Silica Surface Using QCM-D. The alternating adsorptions of β LgA and pectin onto quartz crystal coated with SiO₂ were studied by QCM-D first to confirm the successful assembly of the complex structure at the solid—liquid interface. In order to exclude the effect of β LgA readsorption, instead of incubating the system alternatively with β LgA and pectin, a parallel experiment was conducted by introducing β LgA three times into the QCM chamber. This sample was treated as a negative control. Figure 2a represents a typical QCM-D profile measured from the β LgA/37B pectin system at different overtones, where significant changes in both frequency (ΔF) and dissipation (ΔD) were observed after each surface treatment.

To better understand the QCM-D results, a $\Delta F - \Delta D$ plot was used to present the synchronous changes in frequency and dissipation after each surface treatment.⁴⁵ The $\Delta F - \Delta D$ plots measured from all the β LgA-pectin systems looked similar and demonstrated similar surface deposition mechanisms (Figure S1). Taking the β LgA-SR pectin system as a representative, the

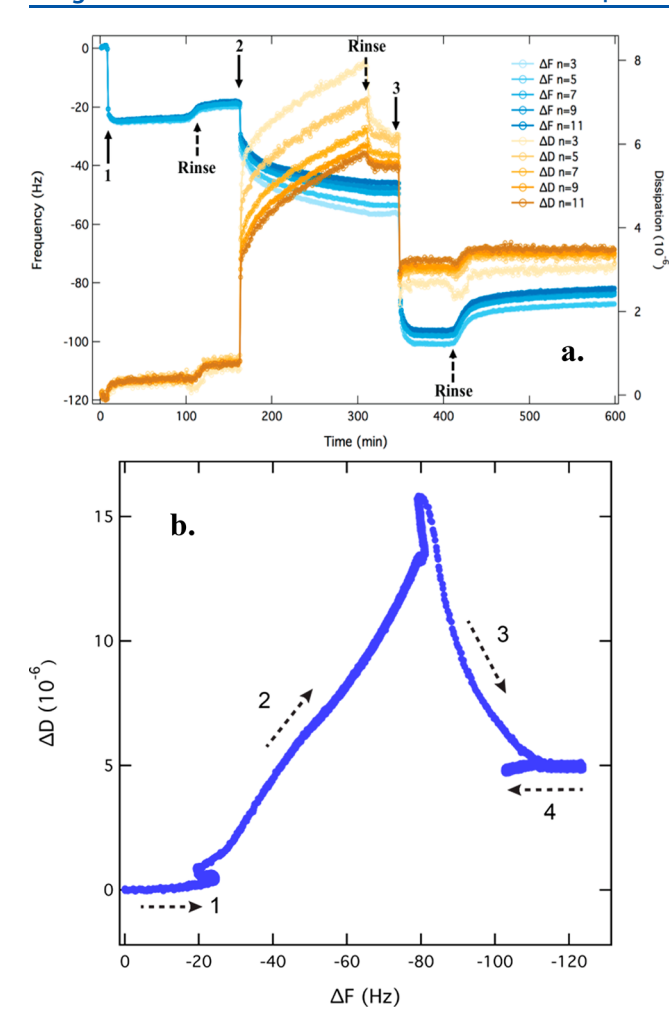


Figure 2. QCM-D profile measurement of β LgA/pectin systems. (a) Typical changes of resonant frequencies (ΔF) and energy dissipations (ΔD) versus time measured during the multiple incubation steps at various overtones. (1) Adsorption of β LgA onto silica surface; (2) deposition of 37B pectin layer to the existing β LgA layer; (3) final β LgA incubation. The QCM chip was rinsed with buffer after each incubation process, as indicated in the graph by the dashed arrows. The letter n represents the overtone number. (b) $\Delta F - \Delta D$ plot from alternative adsorptions of β LgA and 5R pectin onto a silica surface. Steps 1 to 4 denote the four processes during the formation of the LbL assemblies.

direction of $\Delta F - \Delta D$ profile changed after reaching each of the three turning points. It was anticipated that the observed direction change in $\Delta F - \Delta D$ profile was indicative of four mechanistic processes (Figure 2b). The first involved the adsorption of β LgA onto the silica surface, forming a rigid protein layer as evidenced by the minor change in dissipation. Second, incubating the surface with 5R pectin led to a significant increase in dissipation, indicating the formation of a flexible and highly hydrated layer. Third, after incubating the surface with β LgA for a second time, the drop in dissipation suggests the formation of a more rigid and compact surface structure. Finally, the system was washed with buffer to remove loosely bound β LgA, and a slight decrease in mass was observed while the dissipation value remained unchanged.

The measured ΔF and ΔD values for all β LgA-pectin systems are summarized in Figure 3. All systems showed a systematic decrease in frequency and a similar trend in dissipation shifts. The greatest ΔF and ΔD values were

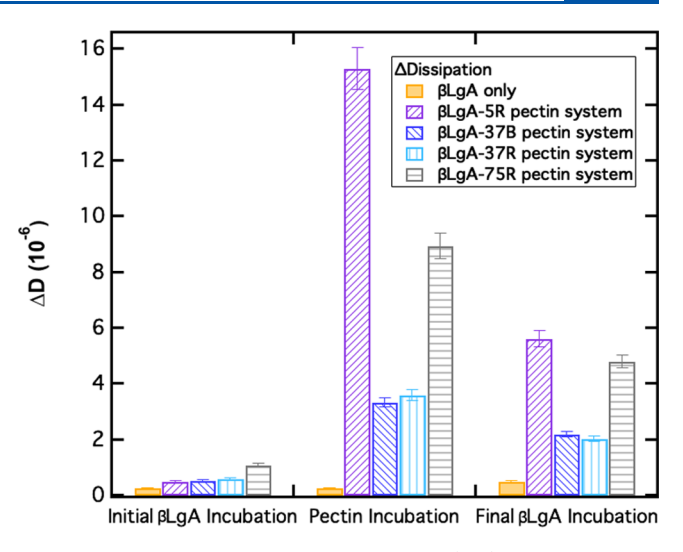


Figure 3. Measured changes in frequency (top) and dissipation (bottom), after each surface treatment for all β LgA-pectin systems. β LgA negative control refers to the sample incubated only with β LgA solution. Error bars represent one standard deviation.

measured for β LgA-5R system, implying that the film structure had more mass and was more viscoelastic than other systems. It is anticipated that the large number of negative charges carried by 5R pectin promoted their adsorption onto the β LgA surface through electrostatic interactions. On the other hand, the large dissipation value observed for the 5R pectin system could have resulted from the electrostatic repulsions among the charged pectin backbones, leading to a more expanded matrix structure. Comparable ΔF and ΔD values were measured for β LgA-37B and β LgA-37R systems, implying that both had similar mass and viscoelastic properties. Compared to 37B and 37R, the 75R pectin has more methyl-esterified GalA groups and therefore a smaller overall charge density. However, more significant changes in frequency and dissipation are observed for the 75R system. The large ΔF and ΔD values recorded for the β LgA-75R system are potentially due to their higher molecular weight and a larger number of noncharged methyl-esterified segments that do not interact with β LgA molecules. Consequently, they would contribute to the surface mass and form a more extended structure, resulting in high dissipation values. 46,47 For the surface that was repeatedly incubated with β LgA (Figure S1), the frequency and dissipation showed very little change after each surface treatment compared to those observed for β LgA-pectin systems.

Sequential β LgA and Pectin Surface Deposition Characterized by NR. After confirming the successful assembly of β LgA-pectin complexes via QCM-D measurements, NR experiments were performed to probe the internal organization of the LbL structure *in situ*. Figure 4 shows a set of NR profiles measured from the β LgA-37B pectin system in D₂O contrast. The measured reflectivity data are plotted as RQ^4 vs Q to increase the visibility of features in the reflectivity profiles. The NR profiles decrease in reflectivity after each addition step, showing successful deposition of protein and polysaccharide onto the silica surface. After the pectin and the second β LgA incubation, Kiessig fringes started to develop, indicating that surface-deposited macromolecules formed a thicker and more well-defined film.

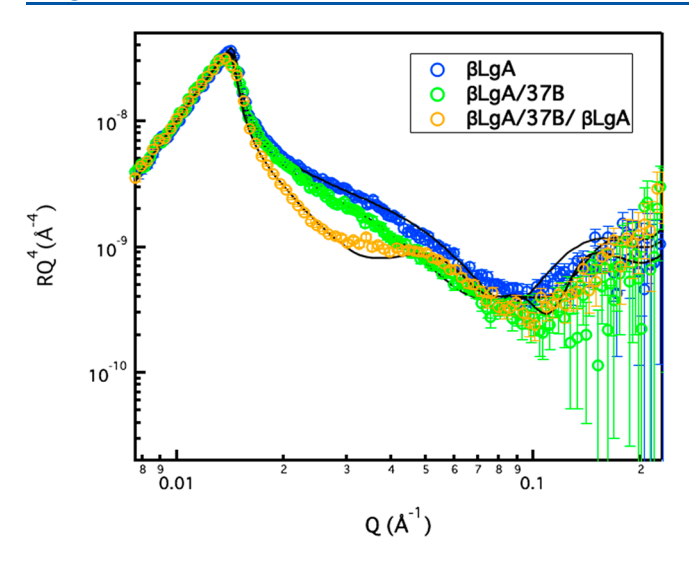


Figure 4. Measured (open circles) and calculated (solid lines) neutron reflectivity profiles obtained from the silicon wafer in D_2O contrast after three consecutive surface treatments, namely βLgA (blue), 37B pectin (green), and βLgA again (orange). Error bars represent standard deviations calculated from the neutron count data.

NR curves measured after β LgA incubation in D₂O and H₂O-based buffer were corefined using a single layer of protein model (Figure S2). A two-protein layers model was also considered; however, the fitting result was much worse, suggesting that β LgA formed a monolayer on the silica surface. The thickness of the adsorbed β LgA layer was 33 \pm 2.0 Å, with a solvent percentage of $64 \pm 4.0 \text{ v/v}$ %. This layer thickness is slightly less than the reported diameter of the globular β LgA protein⁴⁸ (36 Å), implying that a monolayer of β LgA was formed and that the conformation of β LgA changed slightly upon surface adsorption. Based on the fitting result, the surface coverage of β LgA was calculated to be 1.57 \times 10⁻⁷ g/cm² using eq 5, similar to that reported in a previous study by Wahlgren et al. 49 Collectively, results from QCM-D and NR experiments suggest that after the first β LgA incubation, β LgA molecules formed a rigid and compact monolayer on the silica surface, presumably through electrostatic interactions. 50,51

After a stable β LgA monolayer was formed, pectins with different charge patterns were introduced into the sample cell chamber. The reflectivity for each β LgA-pectin system was modeled with a three-layer structure: (1) a layer of SiO₂, (2) a hydrated inner layer of β LgA mixed with pectin, and (3) a hydrated pectin outer layer (Figure 5).

The three-layer model assumed that some charged segments of pectin were able to interact with β LgA through electrostatic interactions (train-like structure), while the other parts of the long chain molecule projected out of the β LgA layer and formed a loose pectin outer layer (loops and tails), as evident by the large dissipation values from QCM-D measurements. Therefore, the mixed β LgA-pectin layers were of comparable thickness to that of the β LgA monolayer alone (Table S2), while the change in nSLD values suggested the incorporation of a certain amount of pectin molecules also in this layer. The outer pectin layer contained only pectin molecules (as evident by the nSLD value) and appeared to be highly hydrated, as expected. Under the studied buffer conditions, pectin molecules and the silica surface were both negatively charged; as a result, the adsorption of pectin onto silica surface was not likely to happen. Indeed, a series of QCM-D experiments were

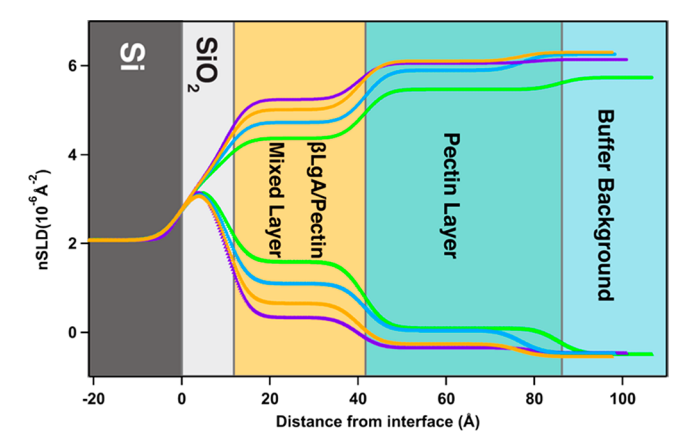


Figure 5. nSLD profiles obtained from NR data fitting for each system after alternative adsorption of βLgA and pectin. Reflectivity data were collected in D2O (curves with nSLD values ranging from $2\times 10^{-6}~{\rm \AA}^{-2}$ to $6\times 10^{-6}~{\rm \AA}^{-2}$) and H2O (curves with nSLD values ranging from $2\times 10^{-6}~{\rm \AA}^{-2}$) and H2O (curves with nSLD values ranging from $2\times 10^{-6}~{\rm \AA}^{-2}$ to $-0.6\times 10^{-6}~{\rm \AA}^{-2}$). Data sets are colored as βLgA -5R pectin (green); βLgA -37B pectin (blue); βLgA -37R pectin (orange); βLgA -75R pectin (purple). Colored background is provided to illustrate the different layers used to fit the NR data.

performed to confirm that pectin molecules did not attach to silica surfaces (results not shown).

Therefore, the internal organization of the LbL assembly was revealed in great detail by fitting the NR data. With the solvent percentage and the known nSLD values of β LgA and pectin molecules, we were able to calculate the volume fractions of both macromolecules using eqs 3 and 4. The estimated volume fraction of β LgA and pectin in each layer is represented in Figure S3. Using the fitted results from NR, we calculated the surface coverage of both macromolecules in each layer using eq 5 (Figure 6). After incubating the surface with pectin solutions,

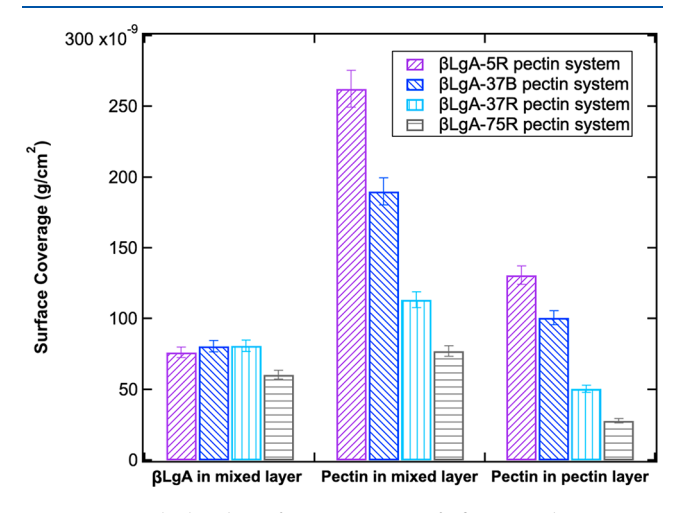


Figure 6. Calculated surface coverage of β LgA and pectin in individual layers after pectin adsorption. Error bars represent $\pm 5\%$ of the derived surface coverage values. Data sets are colored to represent various β LgA-pectin systems.

the amount of β LgA remaining on the surface decreased from $1.57 \times 10^{-7} \text{ g/cm}^2$ to around $0.75 \times 10^{-7} \text{ g/cm}^2$ among all examined β LgA-pectin systems. Such a decrease in surface-bound β LgA could have resulted from repetitive washing and buffer exchange during NR measurements. The amount of pectin attached to the surface demonstrates dependence on the

charge density of the molecule. It is anticipated that the higher the overall charge possessed by pectin, the stronger the electrostatic interactions with β LgA. Therefore, more pectin molecules were attached to surface-bound β LgAs. Since 5R had the highest local charge density, it interacted with β LgA more strongly, resulting in a less solvated matrix structure. For pectins with similar overall charge densities (37B and 37R), blocky pectin with higher local charge density interacted with β LgA more strongly. As a result, the amount of surface-immobilized pectin was greater in the β LgA-37B system. The lowest amount of pectin was found in the β LgA-75R system. This can be explained by the overall low charge carried by 75R compared to other pectin samples. It should also be noted that the more pectins penetrated into the β LgA layer, the less solvated the mixed layer became (Table S2).

After the pectin treatment, the surface was incubated with β LgA again. NR profile measured from each β LgA-pectin system was fitted using a three-layer model first (a SiO₂ layer, a β LgA-pectin mixed layer, and another β LgA layer on top). However, it appeared that the three-layer model was not appropriate to describe the newly formed matrix structure due to the poor fitting quality. Therefore, considering the sequential surface modification steps, a four-layer model was proposed: (1) a uniform SiO₂ layer, (2) a β LgA monolayer mixed with penetrating pectin, (3) a β LgA and pectin mixed layer, and (4) a highly hydrated top layer with sparsely decorated β LgA. The quality of the fitting was significantly improved. Fitting parameters are listed in Table S3.

Although the NR data were better fitted using a four-layer model to account for compositional fluctuations across different layers, the fitted NR results implied that the internal structure of the LbL assembly was generally homogeneous with the presence of two mixed protein—polysaccharide layers: the inner layer adjacent to the silica surface consisting of β LgA monolayer and pectin, and the outer layer containing pectin and newly introduced β LgA molecules (Figure 7). Results in Tables S2 and S3 show that after the final β LgA deposition, the thickness of the inner β LgA-pectin mixed layer remained

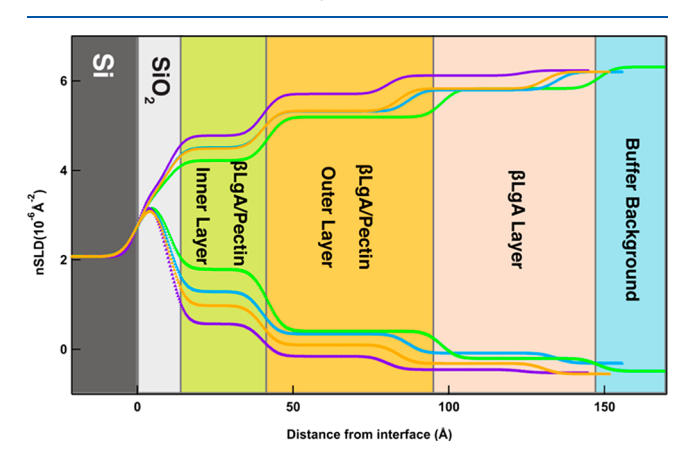


Figure 7. NSLD profiles obtained from NR data fitting for each system after alternative adsorption of βLgA-pectin-βLgA. Reflectivity data was collected in D₂O (curves with nSLD values ranging from 2 × 10^{-6} Å⁻² to 6×10^{-6} Å⁻²) and H₂O (curves with nSLD values ranging from 2 × 10^{-6} Å⁻² to -0.6×10^{-6} Å⁻²). Data sets are colored as βLgA-5R pectin system (green); βLgA-37B pectin system (blue); βLgA-37R pectin system (orange); βLgA-75R pectin system (purple). Colored background is provided to illustrate the different layers used to fit the NR data.

unchanged. The thickness of the outer β LgA-pectin mixed layer increased proportionally with the overall charge density on pectin. The β LgA top layer was highly hydrated with a solvent percentage varied between 87 and 97%, depending on the types of pectin used to form the matrix structure. The thickness of the outer β LgA layer varied between 44 and 50 Å among different systems, consistently greater than the reported diameter of β LgA (around 36 Å⁵²), implying that the β LgA molecules could have formed oligomers/aggregates upon interaction with pectin. This observation is in line with our previous study on β LgA/pectin complexes, where we found that β LgA could form oligomers or β LgA-rich clusters when interacting with pectin molecules in solution. Si

The volume fraction of β LgA and pectin in each layer can be found in Figure S4. The surface coverage of β LgA and pectin in each layer was calculated and represented in Figure 8.

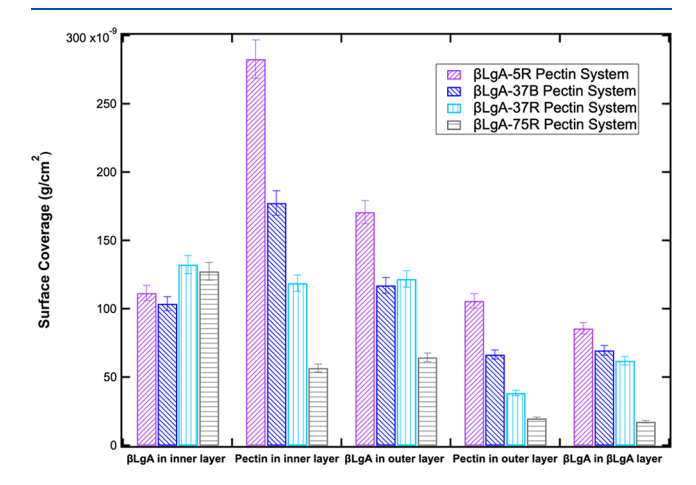


Figure 8. Calculated surface coverage of β LgA and pectin in individual layers after final incubation in β LgA solution. Error bars represent $\pm 5\%$ of the derived surface coverage values. Data sets are colored to represent various β LgA-pectin systems.

Compared to the results shown in Figure 6, it can be seen that the amount of β LgA in the first mixed layer increased in all systems. This implied that after the final surface incubation with β LgA, the β LgA molecules not only interacted with pectin molecules but some penetrated through the complex structures and attached to the silica surface. The readsorption of βLgA may be due to the insufficient coverage on the silica surface. When more β LgA molecules are introduced into the system, they may be able to deposit onto the vacant spots where sufficient negative charges remain on the surface. If we compare all β LgA-pectin systems, we can see that the degree of β LgA readsorption was more significant in 37R and 75R pectin systems. For pectin molecules that are highly charged, the majority of β LgA will be adsorbed onto pectin networks rather than onto the silica surface. Moreover, as the secondary β LgA molecules interact with pectins, the outer β LgA-pectin mixed layer becomes more compact. Therefore, the readsorption of β LgA is hindered by the denser matrix network formed with more charged pectins.

NR results also suggested the presence of a β LgA layer on top of the intertwined β LgA-pectin matrix structure after the final surface treatment with β LgA. The thickness of β LgA layer was greater than the diameter of β LgA monomer, suggesting the possible presence of β LgA oligomers. The solvent percentage of the β LgA layer was as high as 90% (Table

Pectin with High Charge Density

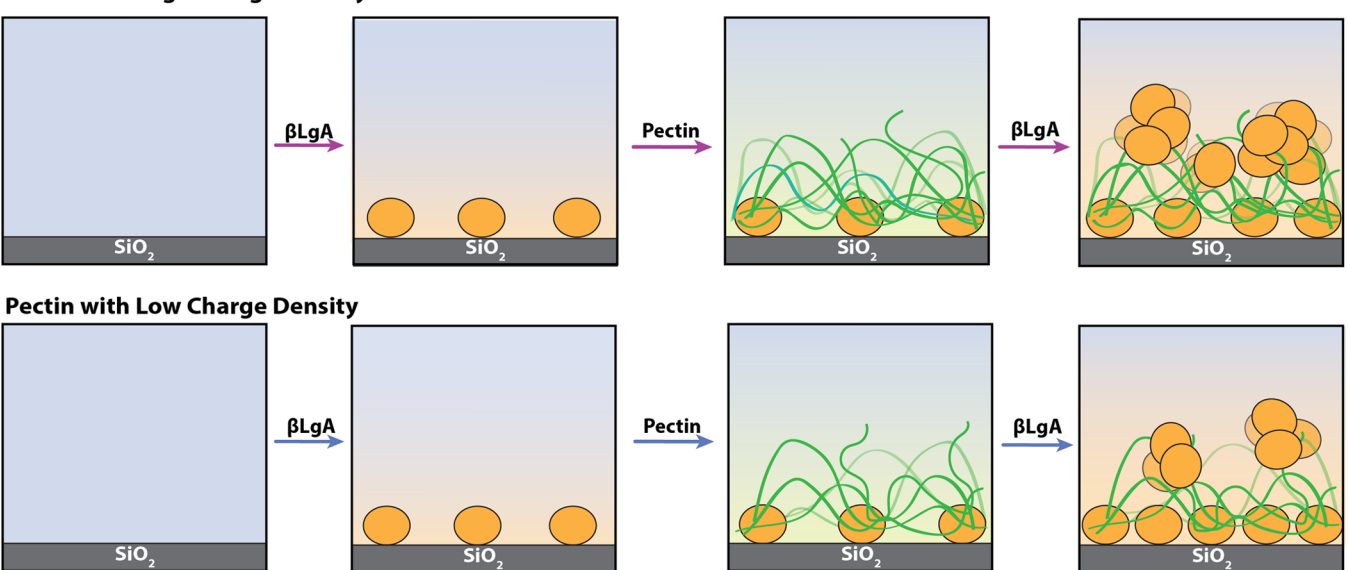


Figure 9. Illustration showing the assembly mechanism and structure of β LgA-pectin complexes formed on silica surface. β LgA molecules are illustrated with orange spheres, while pectins are represented by green curves.

S3), implying that the top surface of the final β LgA/pectin complex structures was decorated with several isolated proteinrich domains. It is also noted that the thickness and density of the β LgA layer were proportional to the overall and local charge densities carried by pectin. Previously, we studied the interactions between β LgA and pectin in solution under the same buffer conditions, i.e., pH 4 with low ionic strength. We found that β LgA underwent considerable conformational changes and formed clusters upon interaction with pectin. 53,54 Therefore, it is anticipated that the last-introduced β LgA molecules interacted with extended pectin segments, and this further led to the nucleated growth of β LgA-rich domains among individual pectin chains. In this case, β LgA aggregates acted as the "cross-linkers" to hold the flexible pectin molecules together, in concordance with the significant decrease in dissipation value (Figure 3). Therefore, in combination with all QCM-D and NR results, we propose an assembly mechanism for the formation of β LgA-pectin complex structures at the solid-liquid interface (Figure 9).

Model System and Characterization Techniques. In this study, β LgA and pectin were chosen as the model protein and polysaccharide, respectively. β LgA is a globular protein that is abundant in bovine milk. The isoelectric point of β LgA is around pH 5.2, below which the proteins are overall positively charged and above which the proteins are negatively charged. Pectin is a charged polysaccharide with a pK_a value of 3.5, above which the pectin molecules are negatively charged. Therefore, in order to promote the electrostatic interactions between β LgA and pectin and ensure the successful assembly of LbL structures, we chose to prepare our samples in pH 4 buffer with low salt, where β LgA and pectin molecules carried positive and negative charges, respectively.

In our study, QCM-D measurements were performed first to ensure that complex structures could be built on silica surfaces in an LbL fashion and that the complex structures were stable in the time frame needed for neutron reflectometry measurements. Since high dissipation values were measured from all β LgA and pectin systems, we used parameters obtained from

NR measurements to quantify the amount of β LgA and pectin molecules in their complex structures formed at the solid—liquid interface.

Assembly Mechanism and Mesoscale Architecture of Protein-polysaccharide Composite Materials Formed at Solid-Liquid Interface. At pH 4, the silanol groups on the silica surface were deprotonated, leaving the surface carrying a negative charge.⁵⁸ Therefore, positively charged β LgA molecules were attached to silica surfaces through mainly electrostatic interactions. NR fitting results also implied that β LgA formed a monolayer on hydrophilic silica surfaces. The adsorption of proteins to charged surfaces has been extensively studied for both fundamental and application purposes. 59-62 In particular, the formation of protein monolayer on silica surfaces has been reported for many proteins including lysozyme, 59 bovine serum albumin, 6 tropoelastin, 63 and β Lg. 64 It is now commonly accepted that as proteins adsorb onto solid surfaces, they are prone to conformational changes, through which their interactions with the surface can be maximized. 65,66 In our study, the thickness of β LgA layer was 33 \pm 2.0 Å, which was slightly smaller than the diameter of a native protein at 36 Å, suggesting that β LgA molecules adopted a slightly compressed conformation upon surface immobilization, facilitating their attachment to the silica surface. The surface-bound β LgA molecules then acted as anchoring points for the subsequent growth of matrix structures.

After incubating the β LgA-covered surface in pectin solutions, two layers of structures with distinct compositions were characterized: a mixed β LgA-pectin layer at the solid–liquid interface and an extended pectin layer on top. Previously, Ettelaie et al. used the self-consistent field (SCF) approach to predict the structure of protein–polysaccharide complexes formed at an interface. Their result suggests that if polysaccharide molecules are homogeneously charged, then one mixed layer of protein–polysaccharide is formed; if polysaccharide molecules are nonuniformly charged, the resulting complex will demonstrate two layers: a mixed protein–polysaccharide layer and an extended pectin layer.

In our study, we used real pectin samples with both charged and noncharged segments that were either randomly or blockwisely distributed along the polymer chain. Therefore, our experimental result is in good agreement with the hypothesis made by Ettelaie et al. that nonuniformly charged polysaccharides will lead to interfacial structures with two distinct layers.

In this study, the surface coverage of β LgA and pectin molecules was calculated from the NR fitting results using eq 5. Changes in surface coverage of β LgA after each surface treatment are shown in Figure S5. The amount of surfacebound β LgA molecules reduced systematically after the second surface treatment, i.e., incubating in pectin solutions and then rinsing. The amount of β LgA molecules that remained surfacebound was consistent across different pectin systems, suggesting that the β LgA molecules might be lost due to several rounds of rinsing (including both washing and buffer exchanging between hydrogenated and deuterated buffer). Therefore, the amount of mass loss did not show dependence on the type of pectins used. After the third surface treatment, the total surface coverage of β LgA in the complex assemblies increased significantly and exceeded its surface coverage reached after the first surface treatment. The surface coverage of β LgA after the third surface treatment increased as overall and local charge density of the pectin molecule increased. Such increase in β LgA surface coverage was anticipated to come from two routes: (1) by interacting with pectin molecules and (2) through readsorption to the silica surface. Different from β LgA, the surface coverage of pectin estimated after the second and third surface treatments remained at a comparable level for the 5R pectin system, suggesting the firm attachment of pectin molecules to the surface-bound β LgA layer. A reduction in pectin surface coverage was observed after the third surface treatment for other pectin systems: the smaller the overall or local charge density carried by pectin, the more significant the mass loss (Figure S5), possibly due to weaker interactions between β LgA and pectin molecules.

It was recognized through fitting the NR data that the final complex assembly formed at the interface has β LgA and pectin molecules intertwined into a matrix structure. Although a fourlayer model was used to fit the NR data after the final surface treatment process, two inner layers are composed of both β LgA and pectin, although with varying solvent percentages and amounts of individual macromolecules. Therefore, although the β LgA and pectin assemblies were prepared in a LbL fashion, the resulting complexes did not exhibit structures with clearly separated β LgA and pectin layers. Instead, a rather homogeneous matrix structure was formed with β LgA and pectin molecules interconnected into a three-dimensional network. Moreover, our results demonstrated that β LgA formed oligomers or β LgA-rich domains as they interact with pectin molecules under the studied buffer conditions. This is in agreement with our previous study, where we characterized the structure of β LgA and pectin complexes formed in solution under the same buffer condition.²¹ It is anticipated that the β LgA-rich domains could act as cross-linkers and bring flexible pectin chains together into a porous network. A previous study by Ganzevles et al. characterized the interfacial structure of β Lg-pectin complexes formed at the air—water interface.⁶⁸ With NR measurements, they found that β Lg molecules formed a monolayer at the interface first. As pectin molecules were added to the system, they not only penetrated into the β Lg monolayer at the interface but also interacted with β Lg

molecules in solution and formed a dense matrix structure beneath the interfacial β Lg-pectin layer. 68 Comparing our result to the study by Ganzevles et al., it can be seen that similar structures were formed when βLg and pectin formed complexes at both air-water and solid-liquid interfaces via a sequential adsorption approach. The study by Ganzevles et al. also mentioned the hampered mobility of β Lg at or in close vicinity to the interface.⁶⁸ Although we did not measure the diffusivity of β LgA molecules within the complex assemblies formed on the silica surface, our results did show that β LgA molecules could go through some level of conformational changes as they were in contact with the silica surface over time. Such conformational change is believed to maximize their contact with the surface. 65 Therefore, the surface-bound β LgA molecules are less mobile. Moreover, β LgA could go through nucleated growth and form clusters when interacting with pectin molecules; therefore, the mobility of β LgA molecules could be further reduced.

Potential Applications and Future Directions. The biological importance of extracellular matrix (ECM) inspired the development of protein-polysaccharide composite materials to be used in biomedical research as artificial tissues or implants. 18,69,70 To better recapitulate the structural and topographical features of ECM, protein-polysaccharide composites are carefully fabricated so that they exhibit similar or improved properties that are critical for the biological functions of ECM. For example, the porosity and density of ECM play significant roles in controlling the mass transfer of chemicals and the proliferation of cells within the matrix structure. Therefore, the ability to tune the interactions and subsequently the hierarchical structure of protein and polysaccharide complex assemblies is critical in developing composite materials for desired applications. In this study, we show that the structure of β LgA-pectin complexes formed via an LbL approach varies with pectin charge properties: the higher the overall and local charge density carried by the pectin, the stronger they interact with β LgA molecules, and subsequently, the denser and less solvated the matrix structures. Therefore, our research demonstrates that the hierarchical structure of protein-polysaccharide composite materials can be controlled and tuned by using polysaccharides with varying charge patterns. Conveniently, polysaccharides with varying charge patterns can be produced either by chemical treatments or more efficiently via enzymatic reactions. 71,72 Our findings will permit the development of protein-polysaccharide composites with desired properties including porosity, density and level of hydration. All these characteristics are important for designing matrix structures that benefit the transportation, adhesion, and proliferation of cells. Moreover, the combined use of QCM-D and NR allows for the in situ characterization of the compositional and architectural changes of biological complexes formed at the solid-liquid interface, representing a unique characterization tool for studying the dynamics and structure of a wide range of model biological systems.

CONCLUSIONS

The viscoelastic property and internal composition of the self-assembled LbL structures formed with β LgA and pectin were characterized by QCM-D and NR. Our results demonstrate that rather than forming a distinct multilayered structure with clear boundaries between individual phases, β LgA and pectin molecules interacted with each other and formed a cohesive

matrix structure at the solid-liquid interface. The final complex structure was featured by surface-bound β LgA molecules as anchoring points for the matrix consisting of intertwined pectin chains that were cross-linked by β LgA-rich clusters. The β LgA/pectin complexes formed at the solid liquid interface exhibited similar structural features to those formed in solution. Our results also show that the density of protein-polysaccharide matrix structure is dependent on the charge properties of polysaccharides; the higher the overall or local charge density possessed by pectin, the denser and less solvated the matrix structure. Hence, the microstructure of protein-polysaccharide complex assemblies can be controlled by using polysaccharides with different charge properties. Such knowledge will benefit the design and development of protein-polysaccharide composite materials with desired properties that can be used for various biomedical applications.

ASSOCIATED CONTENT

5 Supporting Information

The Supporting Information is available free of charge at https://pubs.acs.org/doi/10.1021/acs.langmuir.2c02003.

Dissipation/frequency shift correlation and neutron reflectometry profiles measured from various β LgA and pectin systems; calculated volume fraction of β LgA and pectin in individual layers; changes in total surface coverage of β LgA and pectin after each surface treatment; nSLD values of mixed protein/polysaccharide complex in both D₂O and H₂O contrasts; fitting parameters of neutron reflectivity data (PDF)

AUTHOR INFORMATION

Corresponding Author

Amy Y. Xu — Department of Chemistry, Louisiana State University, Baton Rouge, Louisiana 70803, United States; orcid.org/0000-0002-4071-1750; Email: amyxu@lsu.edu

Authors

Shanta Biswas — Department of Chemistry, Louisiana State University, Baton Rouge, Louisiana 70803, United States; orcid.org/0000-0002-6199-3291

Laurence D. Melton – School of Chemical Sciences, The University of Auckland, Auckland 1142, New Zealand; orcid.org/0000-0002-0166-9414

Andrew R. J. Nelson — Australian Centre for Neutron Scattering, ANSTO, Kirrawee DC, New South Wales 2232, Australia; orcid.org/0000-0002-4548-3558

Anton P. Le Brun — Australian Centre for Neutron Scattering, ANSTO, Kirrawee DC, New South Wales 2232, Australia; orcid.org/0000-0003-2431-6985

Frank Heinrich – Department of Physics, Carnegie Mellon University, Pittsburgh, Pennsylvania 15213, United States; NIST Center for Neutron Research, National Institute of Standards and Technology, Gaithersburg, Maryland 20899, United States

Duncan J. McGillivray — School of Chemical Sciences, The University of Auckland, Auckland 1142, New Zealand; orcid.org/0000-0003-2127-8792

Complete contact information is available at: https://pubs.acs.org/10.1021/acs.langmuir.2c02003

Notes

Certain commercial equipment, instruments, or materials (or suppliers, or software, etc.) are identified in this paper to foster understanding. Such identification implies neither recommendation or endorsement by the National Institute of Standards and Technology nor that the materials or equipment identified are necessarily the best available for the purpose.

The authors declare no competing financial interest.

ACKNOWLEDGMENTS

This work is supported by Bioprocessing and Bioengineering Grant No. 2022-67022-38145 from the USDA National Institute of Food and Agriculture. A.Y.X. also acknowledges the financial support from the National Science Foundation EPSCoR-Louisiana Materials Design Alliance (LAMDA) program (Grant No. OIA-1946231). The authors would also like to thank the Australian Institute of Nuclear Science and Engineering (AINSE Limited) for providing travel support to ANSTO for neutron experiments. ANSTO is thanked for the provision of beamtime. Prof. Jenny Malmstrom from the University of Auckland and Prof. Bill Williams from Massey University are acknowledged for valuable discussions.

REFERENCES

- (1) Scott, J. E. Connective Tissues the Natural Fiber-Reinforced Composite-Material. J. R. Soc. Med. 1983, 76 (12), 993–994.
- (2) Rajeshwar, K.; de Tacconi, N. R.; Chenthamarakshan, C. R. Semiconductor-based composite materials: Preparation, properties, and performance. *Chem. Mater.* **2001**, *13* (9), 2765–2782.
- (3) Fraile-Martinez, O.; Garcia-Montero, C.; Coca, A.; Alvarez-Mon, M. A.; Monserrat, J.; Gomez-Lahoz, A. M.; Coca, S.; Alvarez-Mon, M.; Acero, J.; Bujan, J.; Garcia-Honduvilla, N.; Asunsolo, A.; Ortega, M. A. Applications of Polymeric Composites in Bone Tissue Engineering and Jawbone Regeneration. *Polymers* **2021**, *13* (19), 3429.
- (4) Smith, C. T. G.; Delkowki, M.; Anguita, J. V.; Cox, D. C.; Haas, C.; Silva, S. R. P. Complete Atomic Oxygen and UV Protection for Polymer and Composite Materials in a Low Earth Orbit. *ACS Appl. Mater. Interfaces* **2021**, *13* (5), 6670–6677.
- (5) Park, Y.-G.; Min, H.; Kim, H.; Zhexembekova, A.; Lee, C. Y.; Park, J.-U. Three-dimensional, high-resolution printing of carbon nanotube/liquid metal composites with mechanical and electrical reinforcement. *Nano Lett.* **2019**, *19* (8), 4866–4872.
- (6) Bealer, E. J.; Onissema-Karimu, S.; Rivera-Galletti, A.; Francis, M.; Wilkowski, J.; Salas-de la Cruz, D.; Hu, X. Protein-Polysaccharide Composite Materials: Fabrication and Applications. *Polymers (Basel)* **2020**, *12* (2), 464.
- (7) Corr, S. A.; Shoemaker, D. P.; Toberer, E. S.; Seshadri, R. Spontaneously formed porous and composite materials. *J. Mater. Chem.* **2010**, 20 (8), 1413–1422.
- (8) Novak, B. M.; Auerbach, D.; Verrier, C. Low-density, mutually interpenetrating organic-inorganic composite materials via supercritical drying techniques. *Chem. Mater.* **1994**, *6* (3), 282–286.

(9) Abbasi, S.; Ladani, R.; Wang, C.; Mouritz, A. Improving the

- delamination fatigue resistance of composites by 3D woven metal and composite Z-filaments. Compos. Part A Appl. Sci. 2021, 147, 106440. (10) Gorbatikh, L.; Liu, Q.; Romanov, V.; Mehdikhani, M.; Matveeva, A.; Shishkina, O.; Aravand, A.; Wardle, B.; Verpoest, I.; Lomov, S.Hierarchical design of structural composite materials down to the nanoscale via experimentation and modelling. IOP Conference Series: Materials Science and Engineering; IOP Publishing, 2018; p 012002.
- (11) Bealer, E. J.; Onissema-Karimu, S.; Rivera-Galletti, A.; Francis, M.; Wilkowski, J.; Salas-de la Cruz, D.; Hu, X. Protein-Polysaccharide Composite Materials: Fabrication and Applications. *Polymers* **2020**, 12 (2), 464.

- (12) Rosellini, E.; Zhang, Y. S.; Migliori, B.; Barbani, N.; Lazzeri, L.; Shin, S. R.; Dokmeci, M. R.; Cascone, M. G. Protein/Polysaccharide-Based Scaffolds Mimicking Native Extracellular Matrix For Cardiac Tissue Engineering Applications. *J. Biomed. Mater. Res. Part A* **2018**, 106 (3), 769–781.
- (13) Limoli, D. H.; Jones, C. J.; Wozniak, D. J. Bacterial Extracellular Polysaccharides in Biofilm Formation and Function. *Microbiol. Spectr.* **2015**, *3*, 3 DOI: 10.1128/microbiolspec.MB-0011-2014.
- (14) Duan, B.; Wang, M. Customized Ca-P/PHBV nanocomposite scaffolds for bone tissue engineering: design, fabrication, surface modification and sustained release of growth factor. *J. R. Soc. Interface* **2010**, 7 *Suppl 5*, S615–29.
- (15) Huang, C.; Chen, R.; Ke, Q.; Morsi, Y.; Zhang, K.; Mo, X. Electrospun collagen-chitosan-TPU nanofibrous scaffolds for tissue engineered tubular grafts. *Colloids Surf. B Biointerfaces* **2011**, 82 (2), 307–15.
- (16) Bealer, E. J.; Kavetsky, K.; Dutko, S.; Lofland, S.; Hu, X. Protein and Polysaccharide-Based Magnetic Composite Materials for Medical Applications. *Int. J. Mol. Sci.* **2020**, *21* (1), 186.
- (17) Ahmed, T. A. E.; Dare, E. V.; Hincke, M. Fibrin: A versatile scaffold for tissue engineering applications. *Tissue Eng. Part B Rev.* **2008**, *14* (2), 199–215.
- (18) Rosellini, E.; Zhang, Y. S.; Migliori, B.; Barbani, N.; Lazzeri, L.; Shin, S. R.; Dokmeci, M. R.; Cascone, M. G. Protein/polysaccharide-based scaffolds mimicking native extracellular matrix for cardiac tissue engineering applications. *J. Biomed. Mater. Res., Part A* **2018**, *106* (3), 769–781.
- (19) Li, K.; Li, Y. F.; Wang, X. Y.; Cui, M. K.; An, B. L.; Pu, J. H.; Liu, J. T.; Zhang, B. Y.; Ma, G. J.; Zhong, C. Diatom-inspired multiscale mineralization of patterned protein-polysaccharide complex structures. *Natl. Sci. Rev.* **2021**, 8 (8), nwaa191 DOI: 10.1093/nsr/nwaa191.
- (20) Costa, R. R.; Testera, A. M.; Arias, F. J.; Rodriguez-Cabello, J. C.; Mano, J. F. Layer-by-Layer Film Growth Using Polysaccharides and Recombinant Polypeptides: A Combinatorial Approach. *J. Phys. Chem. B* **2013**, *117* (22), 6839–6848.
- (21) Xu, A. Y.; Melton, L. D.; Ryan, T. M.; Mata, J. P.; Rekas, A.; Williams, M. A. K.; McGillivray, D. J. Effects of polysaccharide charge pattern on the microstructures of beta-lactoglobulin-pectin complex coacervates, studied by SAXS and SANS. *Food Hydrocoll.* **2018**, 77, 952–963.
- (22) Kwon, I. K.; Matsuda, T. Co-electrospun nanofiber fabrics of poly(L-lactide-co-epsilon-caprolactone) with type I collagen or heparin. *Biomacromolecules* **2005**, *6* (4), 2096–105.
- (23) Liu, T.; Wang, Y.; Zhong, W.; Li, B.; Mequanint, K.; Luo, G.; Xing, M. Biomedical Applications of Layer-by-Layer Self-Assembly for Cell Encapsulation: Current Status and Future Perspectives. *Adv. Healthc. Mater.* **2019**, *8* (1), e1800939.
- (24) Silva, J. M.; Reis, R. L.; Mano, J. F. Biomimetic Extracellular Environment Based on Natural Origin Polyelectrolyte Multilayers. *Small* **2016**, *12* (32), 4308–42.
- (25) Tang, Z.; Wang, Y.; Podsiadlo, P.; Kotov, N. A. Biomedical applications of layer-by-layer assembly: from biomimetics to tissue engineering. *Adv. Mater.* **2006**, *18* (24), 3203–3224.
- (26) Lipton, J.; Weng, G.-M.; Röhr, J. A.; Wang, H.; Taylor, A. D. Layer-by-Layer Assembly of Two-Dimensional Materials: Meticulous Control on the Nanoscale. *Matter* **2020**, 2 (5), 1148–1165.
- (27) Rawtani, D.; Agrawal, Y. K. Emerging Strategies and Applications of Layer-by-Layer Self-Assembly. *Nanobiomedicine (Rij)* **2014**, *1*, 8.
- (28) Ai, H.; Jones, S. A.; Lvov, Y. M. Biomedical Applications of Electrostatic Layer-by-layer Nano-assembly of Polymers, Enzymes, and Nanoparticles. *Cell Biochem. Biophys.* **2003**, *39* (1), 23–43.
- (29) Chakravartula, S. S. N.; Soccio, M.; Lotti, N.; Balestra, F.; Dalla Rosa, M.; Siracusa, V. Characterization of Composite Edible Films Based on Pectin/Alginate/Whey Protein Concentrate. *Materials* **2019**, *12* (15), 2454.
- (30) Sperber, B. L.; Cohen Stuart, M. A.; Schols, H. A.; Voragen, A. G.; Norde, W. Overall charge and local charge density of pectin

- determines the enthalpic and entropic contributions to complexation with beta-lactoglobulin. *Biomacromolecules* **2010**, *11* (12), 3578–83.
- (31) Fishman, M. L.; Chau, H. K.; Qi, P. X.; Hotchkiss, A. T.; Garcia, R. A.; Cooke, P. H. Characterization of the global structure of low methoxyl pectin in solution. *Food Hydrocoll.* **2015**, *46*, 153–159.
- (32) Liu, G.; Zhang, G.Basic Principles of QCM-D. In *QCM-D Studies on Polymer Behavior at Interfaces*; Springer Berlin Heidelberg. Berlin, Heidelberg, 2013; pp 1–8.
- (33) Kim, J. T.; Weber, N.; Shin, G. H.; Huang, Q.; Liu, S. X. The Study of β -Lactoglobulin Adsorption on Polyethersulfone Thin Film Surface Using QCM-D and AFM. *J. Food Sci.* **2007**, 72 (4), E214–E221.
- (34) Dixon, M. C. Quartz Crystal Microbalance with Dissipation Monitoring: Enabling Real-Time Characterization of Biological Materials and Their Interactions. *J. Biomol. Technol.* **2008**, *19* (3), 151–158.
- (35) James, M.; Nelson, A.; Holt, S. A.; Saerbeck, T.; Hamilton, W. A.; Klose, F. The multipurpose time-of-flight neutron reflectometer "Platypus" at Australia's OPAL reactor. *Nucl. Instrum. Methods Phys. Res.* **2011**, 632 (1), 112–123.
- (36) Nelson, A. Motofit— integrating neutron reflectometry acquisition, reduction and analysis into one, easy to use, package. *J. Phys. Conf. Ser.* **2010**, 251, No. 012094.
- (37) Parratt, L. G. Surface studies of solids by total reflection of X-rays. *Phys. Rev.* **1954**, 95 (2), 359.
- (38) Abelés, F. In Recherches sur la propagation des ondes électromagnétiques sinusoidales dans les milieux stratifiés; Annales de physique, 1950; pp 706-782.
- (39) Gerelli, Y. In Applications of neutron reflectometry in biology. *EPJ. Web of Conferences*; EDP Sciences, 2020; p 04002.
- (40) Nelson, A. Co-refinement of multiple-contrast neutron/X-ray reflectivity data using MOTOFIT. *J. Appl. Crystallogr.* **2006**, 39 (2), 273–276.
- (41) Heinrich, F. Deuteration in Biological Neutron Reflectometry. *Isotope Labeling of Biomolecules Applications* **2016**, *566*, 211–230.
- (42) Myatt, D.; Clifton, L.Biomolecular Scattering Length Density Calculator; ISIS, 2016. http://psldc.isis.rl.ac.uk/Psldc/ (accessed April 2016).
- (43) Schmidt, I.; Cousin, F.; Huchon, C.; Boué, F.; Axelos, M. A. V. Spatial Structure and Composition of Polysaccharide—Protein Complexes from Small Angle Neutron Scattering. *Biomacromolecules* **2009**, *10* (6), 1346–1357.
- (44) Jachimska, B.; Swiątek, S.; Loch, J. I.; Lewiński, K.; Luxbacher, T. Adsorption effectiveness of β -lactoglobulin onto gold surface determined by quartz crystal microbalance. *Bioelectrochemistry* **2018**, 121, 95–104.
- (45) Zhang, S.; Bai, H.; yang, P. h. Real-Time Monitoring Of Mechanical Changes During Dynamic Adhesion Of Erythrocytes To Endothelial Cells By QCM-D. *Chem. Commun.* **2015**, *51* (57), 11449–11451.
- (46) Konradi, R.; Textor, M.; Reimhult, E. Using complementary acoustic and optical techniques for quantitative monitoring of biomolecular adsorption at interfaces. *Biosensors (Basel)* **2012**, 2 (4), 341–76.
- (47) Salas, C.; Rojas, O. J.; Lucia, L. A.; Hubbe, M. A.; Genzer, J. Adsorption of Glycinin and beta-Conglycinin on Silica and Cellulose: Surface Interactions as a Function of Denaturation, pH, and Electrolytes. *Biomacromolecules* **2012**, *13* (2), 387–396.
- (48) Adams, J. J.; Anderson, B. F.; Norris, G. E.; Creamer, L. K.; Jameson, G. B. Structure of Bovine Beta-lactoglobulin (Variant A) At Very Low Ionic Strength. *J. Struct. Biol.* **2006**, *154* (3), 246–254.
- (49) Wahlgren, M.; Arnebrant, T. Adsorption of β -lactoglobulin onto silica, methylated silica, and polysulfone. *J. Colloid Interface Sci.* **1990**, 136 (1), 259–265.
- (50) Norde, W.; Anusiem, A. C. I. Adsorption, desorption and readsorption of proteins on solid surfaces. *Colloids Surf.* **1992**, *66* (1), 73–80.
- (51) Kortesuo, P.; Ahola, M.; Kangas, M.; Jokinen, M.; Leino, T.; Vuorilehto, L.; Laakso, S.; Kiesvaara, J.; Yli-Urpo, A.; Marvola, M.

- Effect of synthesis parameters of the sol-gel-processed spray-dried silica gel microparticles on the release rate of dexmedetomidine. Biomaterials 2002, 23 (13), 2795-2801.
- (52) Goulding, D. A.; Fox, P. F.; O'Mahony, J. A.Chapter 2 Milk proteins: An overview. In Milk Proteins, 3rd ed.; Boland, M., Singh, H., Eds.; Academic Press, 2020; pp 21-98.
- (53) Xu, A. Y.; Melton, L. D.; Ryan, T. M.; Mata, J. P.; Rekas, A.; Williams, M. A. K.; McGillivray, D. J. Effects of polysaccharide charge pattern on the microstructures of β -lactoglobulin-pectin complex coacervates, studied by SAXS and SANS. Food Hydrocoll. 2018, 77,
- (54) Xu, A. Y.; Melton, L. D.; Jameson, G. B.; Williams, M. A. K.; McGillivray, D. J. Structural mechanism of complex assemblies: characterisation of beta-lactoglobulin and pectin interactions. Soft Matter 2015, 11 (34), 6790-6799.
- (55) Brownlow, S.; Morais Cabral, J. H.; Cooper, R.; Flower, D. R.; Yewdall, S. J.; Polikarpov, I.; North, A. C.; Sawyer, L. Bovine betalactoglobulin at 1.8 A resolution-still an enigmatic lipocalin. Structure **1997**, 5 (4), 481–95.
- (56) O'Mahony, J. A.; Fox, P. F.Chapter 2 Milk: An Overview. In Milk Proteins, 2nd ed.; Singh, H., Boland, M., Thompson, A., Eds.; Academic Press: San Diego, 2014; pp 19-73.
- (57) Strom, A.; Schuster, E.; Goh, S. M. Rheological characterization of acid pectin samples in the absence and presence of monovalent ions. Carbohydr. Polym. 2014, 113, 336-343.
- (58) Mathe, C.; Devineau, S.; Aude, J. C.; Lagniel, G.; Chedin, S.; Legros, V.; Mathon, M. H.; Renault, J. P.; Pin, S.; Boulard, Y.; Labarre, J. Structural determinants for protein adsorption/nonadsorption to silica surface. PLoS One 2013, 8 (11), e81346.
- (59) Kubiak-Ossowska, K.; Cwieka, M.; Kaczynska, A.; Jachimska, B.; Mulheran, P. A. Lysozyme adsorption at a silica surface using simulation and experiment: effects of pH on protein layer structure. Phys. Chem. Chem. Phys. 2015, 17 (37), 24070-24077.
- (60) Park, H.; Ma, G. J. R.; Yoon, B. K.; Cho, N. J.; Jackman, J. A. Comparing Protein Adsorption onto Alumina and Silica Nanomaterial Surfaces: Clues for Vaccine Adjuvant Development. Langmuir 2021, 37 (3), 1306–1314.
- (61) Fragneto, G.; Thomas, R. K.; Rennie, A. R.; Penfold, J. Neutron reflection study of bovine beta-casein adsorbed on OTS selfassembled monolayers. Science 1995, 267 (5198), 657-60.
- (62) Hartvig, R. A.; van de Weert, M.; Ostergaard, J.; Jorgensen, L.; Jensen, H. Protein Adsorption at Charged Surfaces: The Role of Electrostatic Interactions and Interfacial Charge Regulation. Langmuir 2011, 27 (6), 2634-2643.
- (63) Le Brun, A. P.; Chow, J.; Bax, D. V.; Nelson, A.; Weiss, A. S.; James, M. Molecular Orientation of Tropoelastin is Determined by Surface Hydrophobicity. Biomacromolecules 2012, 13 (2), 379-386.
- (64) Marsh, R.; Jones, R.; Sferrazza, M.; Penfold, J. Neutron reflectivity study of the adsorption of β -lactoglobulin at a hydrophilic solid/liquid interface. J. Colloid Interface Sci. 1999, 218 (1), 347-349.
- (65) Rabe, M.; Verdes, D.; Seeger, S. Understanding protein adsorption phenomena at solid surfaces. Adv. Colloid Interface Sci. 2011, 162 (1), 87-106.
- (66) Norde, W. Adsorption of proteins from solution at the solidliquid interface. Adv. Colloid Interface Sci. 1986, 25 (4), 267-340.
- (67) Ettelaie, R.; Akinshina, A.; Maurer, S. Mixed proteinpolysaccharide interfacial layers: effect of polysaccharide charge distribution. Soft Matter 2012, 8 (29), 7582-7597.
- (68) Ganzevles, R. A.; Fokkink, R.; van Vliet, T.; Cohen Stuart, M. A.; de Jongh, H. H. J. Structure of mixed β -lactoglobulin/pectin adsorbed layers at air/water interfaces; a spectroscopy study. J. Colloid Interface Sci. 2008, 317 (1), 137-147.
- (69) Ng, J. Y.; Obuobi, S.; Chua, M. L.; Zhang, C.; Hong, S. Q.; Kumar, Y.; Gokhale, R.; Ee, P. L. R. Biomimicry of microbial polysaccharide hydrogels for tissue engineering and regenerative medicine - A review. Carbohydr. Polym. 2020, 241, 116345.
- (70) Chantre, C. O.; Gonzalez, G. M.; Ahn, S.; Cera, L.; Campbell, P. H.; Hoerstrup, S. P.; Parker, K. K. Porous Biomimetic Hyaluronic Acid and Extracellular Matrix Protein Nanofiber Scaffolds for

- Accelerated Cutaneous Tissue Repair. ACS Appl. Mater. Interfaces **2019**, 11 (49), 45498–45510.
- (71) Kaczmarek, M. B.; Struszczyk-Swita, K.; Li, X.; Szczesna-Antczak, M.; Daroch, M. Enzymatic Modifications of Chitin, Chitosan, and Chitooligosaccharides. Front. Bioeng. Biotechnol. 2019, 7, 243.
- (72) Chen, J.; Liu, W.; Liu, C. M.; Li, T.; Liang, R. H.; Luo, S. J. Pectin modifications: a review. Crit. Rev. Food Sci. Nutr. 2015, 55 (12), 1684-98.

□ Recommended by ACS

Modular Platform of Carbohydrates-modified **Supramolecular Polymers Based on Dendritic Peptide Scaffolds**

Long Li, Guosong Chen, et al.

AUGUST 24, 2022 ACS POLYMERS AU

Glycosaminoglycan Mimetic Precision Glycomacromolecules with Sequence-Defined Sulfation and Rigidity Patterns

Miriam Hoffmann, Laura Hartmann, et al.

AUGUST 12, 2022

BIOMACROMOLECULES

READ **C**

Crowded Environment Regulates the Coacervation of Biopolymers via Nonspecific Interactions

Qingwen Bai, Dehai Liang, et al.

DECEMBER 13, 2022

BIOMACROMOLECULES

RFAD 17

Glycopolymers for Drug Delivery: Opportunities and **Challenges**

Martina H. Stenzel.

JUNE 08, 2022

MACROMOLECULES

READ **C**

Get More Suggestions >